CMS Physics Analysis Summary

Contact: cms-pag-conveners-susy@cern.ch 2014/08/12

Search for supersymmetry in two-photons+jet events with razor variables in pp collisions at $\sqrt{s} = 8$ TeV

The CMS Collaboration

Abstract

A search for supersymmetry in pp collisions, in events with at least two photons and one jet, is presented. The dataset, collected at a center-of-mass energy $\sqrt{s} = 8$ TeV in 2012, corresponds to an integrated luminosity of 19.7 fb^{-1}. The signal is characterized as a peak on a falling background in the razor kinematic variable M_R, for events in the tail of the razor ratio R^2. The observed event distribution in M_R is compatible with the prediction derived by the events with small values of R^2. This result is interpreted as an exclusion limit on a set of simplified model spectra for squarks and gluinos, inspired by the phenomenology of gauge-mediated supersymmetry breaking.

1 Introduction

The existence of supersymmetry (SUSY) [1–9] at the electro-weak energy scale is postulated to extend the standard model (SM) of particle physics, such that the mass of the lightest Higgs boson is stabilized, canceling the divergent quantum corrections from fermionic loops with the equivalent contributions from bosonic super partners, and vice versa. Assuming R-parity conservation, only even numbers of SUSY particles can be produced at particle accelerators, the lightest SUSY partner (LSP) being stable. SUSY must be a broken symmetry since SUSY partners degenerate with SM particles have not been observed. Among the several SUSY breaking mechanisms proposed, General Gauge Mediated (GGM) supersymmetry breaking [10–18] provides an interesting phenomenology for proton-proton collisions at the Large Hadron Collider (LHC). In particular, many GGM models predict that the gravitino $\widetilde{\mathrm{G}}$ and the neutralino $\widetilde{\chi}$ are the LSP and the next-to-lightest supersymmetric particle (NLSP), respectively.

In this note, we concentrate on final states containing at least two prompt photons and one jet, originating from the cascade decay of squarks and gluinos to a pair of $\widetilde{\chi}$ and jets, with $\widetilde{\chi}$ decaying to $\widetilde{\mathrm{G}}\gamma$. The events will also have missing transverse energy ($E_{\mathrm{T}}^{\mathrm{miss}}$) due to the LSP $\widetilde{\mathrm{G}}$. We consider pp collisions collected by the Compact Muon Solenoid (CMS) detector at the LHC in 2012, at a center-of-mass energy $\sqrt{s} = 8\,\mathrm{TeV}$. The dataset presented here corresponds to an integrated luminosity of $L = 19.7\ \mathrm{fb}^{-1}$.

In a previous CMS study [19], this SUSY signature was searched for by studying events with large $E_{\mathrm{T}}^{\mathrm{miss}}$ in $4.0\,\mathrm{fb}^{-1}$ of $\sqrt{s} = 8\,\mathrm{TeV}$ data. No evidence for a signal was found and GGM models with production cross section larger than $\approx 10\ \mathrm{fb}^{-1}$ were excluded. A more recent ATLAS study searching for GGM SUSY signatures in two-photon+$E_{\mathrm{T}}^{\mathrm{miss}}$ events in $20.3\,\mathrm{fb}^{-1}$ of $\sqrt{s} = 8\,\mathrm{TeV}$ data set lower limits on gluino and wino masses of 1280 GeV and 570 GeV, respectively, for bino masses above 50 GeV [20].

In this updated study, the two-photon+jet+$E_{\mathrm{T}}^{\mathrm{miss}}$ topology is investigated in a purely data-driven way using the razor variables [21, 22] $\mathrm{M_R}$ and R^2, characterizing the signal as a wide excess in $\mathrm{M_R}$ emerging above the falling SM background, for events populating the tail of the R^2 distribution. The background $\mathrm{M_R}$ shape is determined in a control region of the ($\mathrm{M_R}$, R^2) plane and extrapolated to the tail of R^2. This data-driven background estimate is tested on a control sample of events with calorimetric deposits from hadrons, misidentified as photons. By using R^2, it is possible to extend the study in Ref. [19], accessing events with large R^2 but lower $E_{\mathrm{T}}^{\mathrm{miss}}$.

The observed data distribution in the signal region is found to be in agreement with the predicted background distribution. The result is interpreted in a set of simplified model spectra (SMS) [23–26], inspired by the GGM models.

2 Event selection

The events selected in this study are required to have at least one high-quality reconstructed interaction vertex. If more than one vertex is found, the one with the highest associated $\sum_{\mathrm{track}} p_{\mathrm{T}}^2$, where p_{T} is transverse momentum, is selected and used in the global event reconstruction. A set of detector- and beam-related cleaning algorithms is applied to remove events with detector noise, which would fake signal-like events with high energy and large $E_{\mathrm{T}}^{\mathrm{miss}}$.

Events are collected using the resonant and non-resonant triggers utilized by the higgs to two photon analysis [27]. The triggers use complementary photon selections. One selection re-

quires a loose calorimetric identification based on the shape of the electromagnetic shower and loose isolation requirements on the photon candidates, while the other requires only that the photon have a high value of the shower shape variable R_9. The photons are required to have transverse energy of 26 (18) GeV and 36 (22) GeV on the leading (trailing) photon for the resonant and non-resonant trigger respectively. The effect of the mass cut on non-resonant photons in the intermediate range is found to be less than 1 percent for the targeted signals.

The event reconstruction is performed using the particle flow (PF) algorithm [28], which combines the information of the various detector components in a coherent view of the detected process. Individual particles are reconstructed and classified in five categories: muons, electrons, photons, charged hadrons, and neutral hadrons.

Photons are identified applying a set of loose requirements on isolation and energy cluster shape [29]. At least two photons are required in the event, the highest-p_T (second highest-p_T) photon having $p_T > 30$ (22) GeV. Photons are also required to be within the fiducial region of the tracker ($|\eta| < 2.5$).

The reconstructed PF candidates are clustered using the anti-k_T [30] algorithm, with jet size set to $R = 0.5$, using FASTJET [31]. Jets are selected with $p_T > 40$ GeV and $|\eta| < 2.5$, with each jet required to have a distance $\Delta R = \sqrt{(\Delta\eta)^2 + (\Delta\phi)^2} > 0.5$ from each identified photon. In order to remove jets due to detector noise, jets are required to have at least two constituents. In addition, the fraction of transverse momentum associated with each PF-candidate category (hadronic, neutral hadronic, etc) is required to be < 0.99. At least one jet passing the above criteria is required in each event.

3 Analysis strategy

The razor approach to SUSY event reconstruction aims to approximate the rest frame of the pair-produced SUSY partners. The razor variables were proposed to describe the two-jet topology resulting from the production of two squarks, each decaying to a quark and the LSP, assumed to be a stable neutralino $\widetilde{\chi}_1^0$ [21, 22].

Given a two-jet event, M_R is defined as:

$$M_R \equiv \sqrt{(|\vec{p}_{j_1}| + |\vec{p}_{j_2}|)^2 - (p_z^{j_1} + p_z^{j_2})^2}\,, \tag{1}$$

where $\vec{p}_{j_i}$, $\vec{p}_T^{\,j_i}$, and $p_z^{j_i}$ are the momentum of the ith-jet, its transverse component, and its longitudinal component, respectively. The transverse momentum imbalance in the event is quantified by the variable M_T^R, defined as

$$M_T^R \equiv \sqrt{\frac{E_T^{miss}(p_T^{j_1} + p_T^{j_2}) - \vec{E}_T^{miss}\cdot(\vec{p}_T^{\,j_1} + \vec{p}_T^{\,j_2})}{2}}\,, \tag{2}$$

where E_T^{miss} and pt_i^j are the magnitude of $\vec{E}_T^{miss}$ and $\vec{p}_T^{\,j_i}$, respectively. For $\widetilde{q}$ pair production with $\widetilde{q} \to \widetilde{\chi}_1^0 q$, the distribution of M_R peaks at

$$M_\Delta = (m_{\widetilde{q}}^2 - m_{\widetilde{\chi}_1^0}^2)/m_{\widetilde{q}}\,, \tag{3}$$

where m_p is the mass of a particle p. For the same events, M_T^R has a kinematic edge at M_Δ. The razor ratio R is defined as

$$R \equiv \frac{M_T^R}{M_R}\,. \tag{4}$$

For longer decay chains, as those considered in this study, the M_R distribution becomes wider, but the qualitative features of the M_R and R are retained.

In order to compute the values of M_R and R for generic two-photon+jets+E_T^{miss} events, we consider the set of reconstructed jets and photons in the event. The items of this set are grouped in two exclusive groups, referred to as "megajets". The four-momentum of a megajet is computed as the vectorial sum of the four-momenta of its constituents. Among all the possible megajet pairs in an event, we select the megajet pair with the smallest sum of squared invariant masses. Although the two photons of the event are not explicitly required to be in different megajets, they are nonetheless predominantly placed in opposite megajets. For the samples considered, the photons are always placed in opposite megajets in more than 80 % of events depending on the specific model point with a mode of 99 % (86%) for the T5gg (GGM) samples. It is found that when the photons are not placed in opposite hemispheres, the corresponding change in M_R is at most 15%. Isolated leptons which pass the jet identification criteria can enter the hemisphere clustering as jets. Events with isolated leptons failing the jet identification criteria are clustered without including the jet associated with the lepton. Additionally, all jets are required to be well separated from the two photons to be included in the clustering.

The (M_R, R^2) plane is divided in two different regions: i) a signal region, containing events with $M_R > 600$ GeV and $R^2 > 0.02$; ii) a control region, defined by requiring $M_R > 600$ GeV and $0.01 < R^2 \leq 0.02$. The control region is defined such that any potential signal contamination is less than 10% of the expected number of signal events ($\sigma \times L$) and thus has a negligible bias on the determination of the background shape which is at worst 1-2% for a signal of size $\sigma \times L \approx 20$.

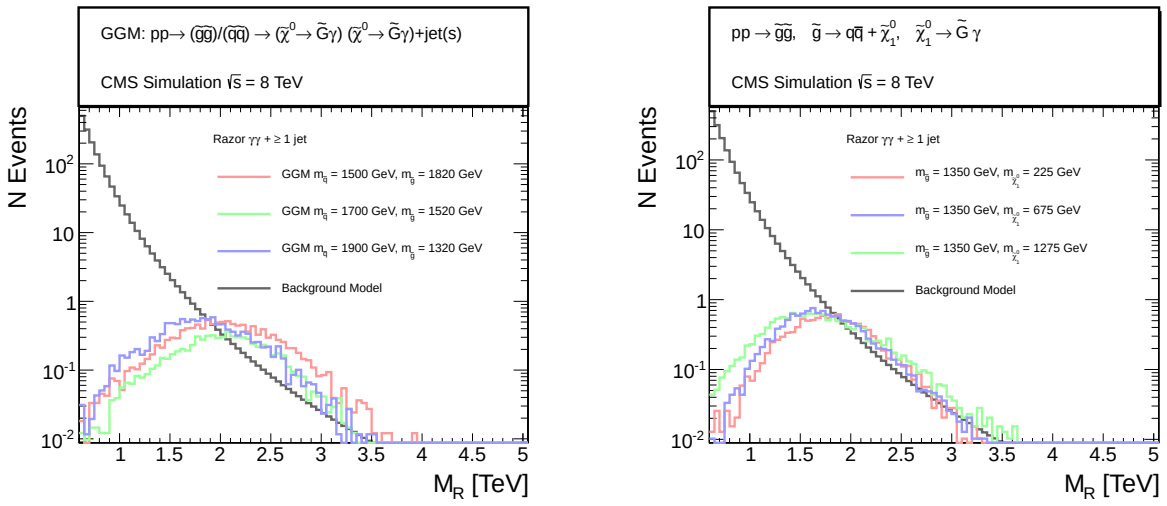

(a) (b)

Figure 1: Signal vs. Background distributions in M_R for the two interpretations: (a) squark-gluino model (b) T5gg model. The background model is normalized to the number of events in the signal region. The signal points are normalized to integrated luminosity times selection efficiency times theoretical cross section.

4 Background prediction and validation

A maximum likelihood fit of the M_R data distribution in the control region is performed, using the functional form

$$P(M_R) \propto e^{-k(M_R - M_R^0)^{\frac{1}{n}}} \quad (5)$$

where M_R^0 is an offset parameter, k quantifies the slope of the 1D distribution in the exponential limit and n describes a deviation from an exponential fall. The parameters obtained are used to describe M_R in the signal region, fixing the overall normalization of the control region fit to the observed yield in the signal region. The covariance matrix derived from the fit in the control region is derived to sample an ensemble of alternative M_R background shapes. For each bin of the M_R distribution, a probability distribution for the yield is derived. A 68% probability range is computed for each yield distribution, using the probability density as ordering principle.

The method is tested using a control sample of jets misidentified as photons, obtained by selecting photon candidates which fail the cluster-shape selection or the isolation requirement, while keeping the rest of the photon selection unaltered (fake-fake sample). In Fig 2 (a) and (b) we show the fit result in the control region and the extrapolation to the signal region, respectively. From previous studies [22], one would expect the M_R shapes in the control region and the signal region to be different, due to the different lower threshold applied to define the two regions. These tests shows that the choice of using a narrow control region makes the distortion of the M_R distribution negligible. The influence of potential backgrounds with real E_T^{miss} (such as $t\bar{t}$ or $W\gamma$) on the method has been investigated using simulation and has been found to be small and well contained within the systematic uncertainty assigned to the method.

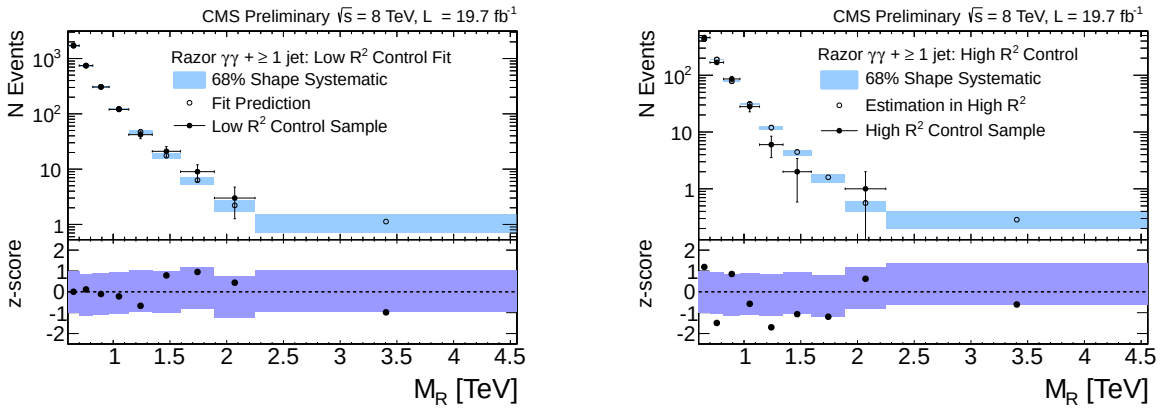

(a) (b)

Figure 2: Data distribution for M_R in the fake-fake control sample (a) in the control region and (b) in the signal region. For each M_R bin, the data (filled dots) are compared to the 68% range obtained from the fit in the control region and extrapolated to the signal region, represented by the blue outlined band. The empty dots represent the center of the 68% range. The bottom panel of each figure gives the z-score (number of gaussian standard deviations) comparing the filled dots to the band. The purple band shows the position of the 68% window about the expected value.

A signal originating from heavy squarks or gluinos would result in an wide bump emerging in the M_R distribution. This is shown in Fig. 3, where a signal sample of squarks and gluinos, with masses set respectively to $m_{\tilde{q}} = 1400$ GeV and $m_{\tilde{g}} = 1820$ GeV and the production cross section $\sigma = 2.7$ fb, is added to the fake-fake sample. The signal contamination is negligible in

the control region and it does not change the background shape of Fig. 2 (a). On the other hand, the extrapolation would not account for the excess in the tail in the presence of signal.

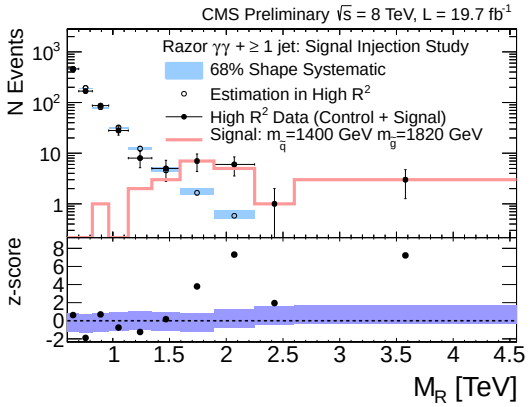

Figure 3: Data distribution for M_R in a sample of fake-fake data events and injected with simulated squark and gluino events. Squark and gluino masses are set to $m_{\tilde{q}} = 1400$ GeV and $m_{\tilde{g}} = 1820$ GeV respectively, and the production cross section is fixed to $\sigma = 2.7$ fb. The signal contribution is shown by the red histogram. For each M_R bin, the data (filled dots) are compared to the 68% range obtained from the fit in the control region and extrapolated to the signal region, represented by the blue outlined band. The empty dots represent the center of the 68% range. The bottom panel of each figure gives the z-score (number of gaussian standard deviations) comparing the filled dots to the band. The purple band shows the position of the 68% window about the expected value. .

5 Systematic uncertainty

The systematic uncertainty in the background data-driven method originates from the fit uncertainty in the control region. The uncertainty is quantified in each M_R bin from the yield distribution derived from an ensemble of background shapes, sampled from the fit covariance matrix. The jet energy corrections contribute to the systematic uncertainty on the signal distribution. The knowledge of the parton density functions and the integrated luminosity contribute to the uncertainty on the signal normalization.

The typical size of each contribution is summarized in Table 1. The shape systematics on the background are determined bin by bin with smaller systematics where the fit shape is constrained (in lower M_R bins) , and larger where uncertainy in the fit parameters accomodate larger deviations in the expected number of events (higher M_R bins). The percentage listed is to be interpreted as the fractional value of the expectation equivalent to a single guassian standard deviation. The fit shape systematic corresponds to uncertainty in the parameters in the fit. The fit function systematic estimates our uncertainty due to the choice of fit function and the differences between the control and signal region functional form. The background systematics dominante the uncertainty for the cross section upper limit interpretation.

The systematics on the signal are subdominant and are determined bin by bin if listed as shape. Systematics not listed as shape are flatly applied to the signal normalization (luminosity, trigger efficiency, signal rate, acceptance). Photon MC/Data systematics are applied to correct for known differences between the MC and Data event by event. Jet energy scale correction systematics apply to number of events in a given M_R bin. By varying the jet energy scale we

Background systematic	Value
Fit shape	shape (bin by bin) 4 - 40%
Fit function systematic	shape (bin by bin) 5 - 50%

Signal systematic	Value
Data/MC photon scale factors	1-2%
Trigger efficiency	1%
Luminosity	2.6%
Jet energy scale corrections	shape (bin by bin) 2-5%

Signal Specific Systematics	Squark-Gluino	T5gg
Acceptance due to PDF	1-3%	1%
Signal rate due to PDF	1.0 - 50%	included in SMS xsec error

Table 1: Typical size of the signal and background systematic uncertainties on shape and normalization.

induce a change in the shape of the signal M_R resonance. The percent listed corresponds to the percentage change in the M_R expectation due to a 1 guassian standard deviation modification up or down in the jet energy scale.

6 Results

The background-prediction method described in Section 4 is applied to the events selected by the requirements described in Section 2. Figure 4 (a) shows the fit output and the associated uncertainty band, compared to the data in the control region. The fit result is then used to derive the background prediction in the signal region. The comparison of the prediction to the observed data distribution is shown in Figure 4 (b). No evidence for a signal is found. The largest positive and negative deviation from the predictions are observed for $M_R \approx 2.3$ TeV and $1.1 \lesssim M_R \lesssim 1.9$ TeV, respectively, each corresponding to a local significance of ≈ 1.5 standard deviations.

7 Interpretation

The result is interpreted in two GGM-inspired SMS scenarios:

- **Squark-gluino model:** squark and gluino production including all flavors except the right-handed up-type, with the $\widetilde{\chi}_1^0$ mass fixed at 375 GeV. The $\widetilde{\chi}_1^0 \to \widetilde{G}\gamma$ decay occurs with branching ratio 100%. All other SUSY particles are decoupled with masses set to 5 TeV.
- **Simplified model T5gg:** gluino pair-production, with gluinos decaying to $q\bar{q}\widetilde{\chi}_1^0$, and $\widetilde{\chi}_1^0 \to \widetilde{G}\gamma$. All decays occur with branching ratio 100%.

In both models the gravitino mass is negligibly small ≈ 1 GeV. The corresponding Feynman diagrams for gluino-gluino and squark-squark production are shown in Fig. 5.

Events for T5gg are generated with MADGRAPH V5, in association with up to two partons. The SUSY particles are decayed in PYTHIA6 assuming a flat matrix element. The event is showered in PYTHIA6 and matched to the matrix-element kinematic configuration using the MLM

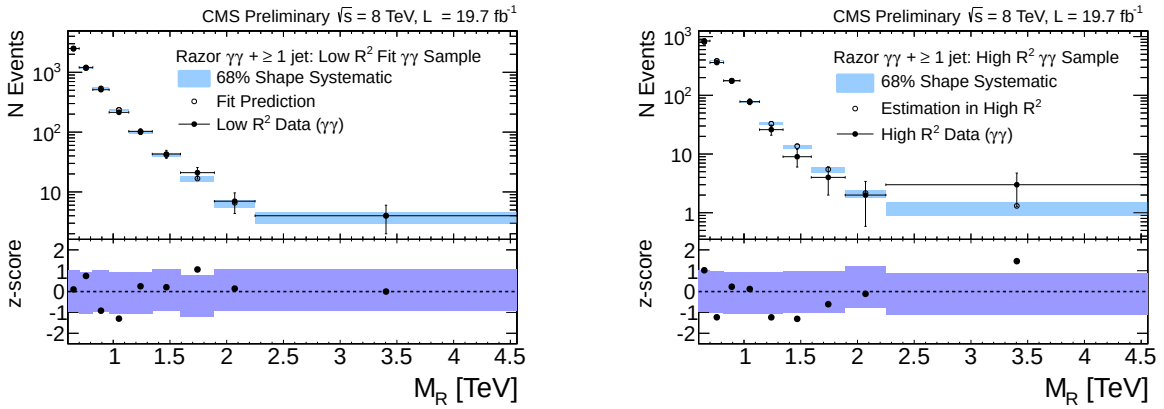

(a) (b)

Figure 4: Data distribution for M_R in the data (a) control region and (b) signal region. For each M_R bin, the data (filled dots) are compared to the 68% range obtained from the fit in the control region and extrapolated to the signal region, represented by the colored band. The empty dots represent the center of the 68% range. The bottom panel of each figure gives the z-score obtained comparing the filled dots to the band. The purple band shows the position of the 68% window about the expected value.

algorithm [32] before being processed through a fast simulation of the CMS detector [33]. The gluino production production cross sections for T5gg is calculated to NLO and next-to-leading-logarithm (NLL) accuracy [34–38], assuming the decoupling of the other SUSY partners. The NLO+NLL cross section and the associated theoretical uncertainty [39] are taken as a reference to derive exclusion limits on SUSY particle masses. The corresponding information for the squark-gluino model is given in Ref. [19].

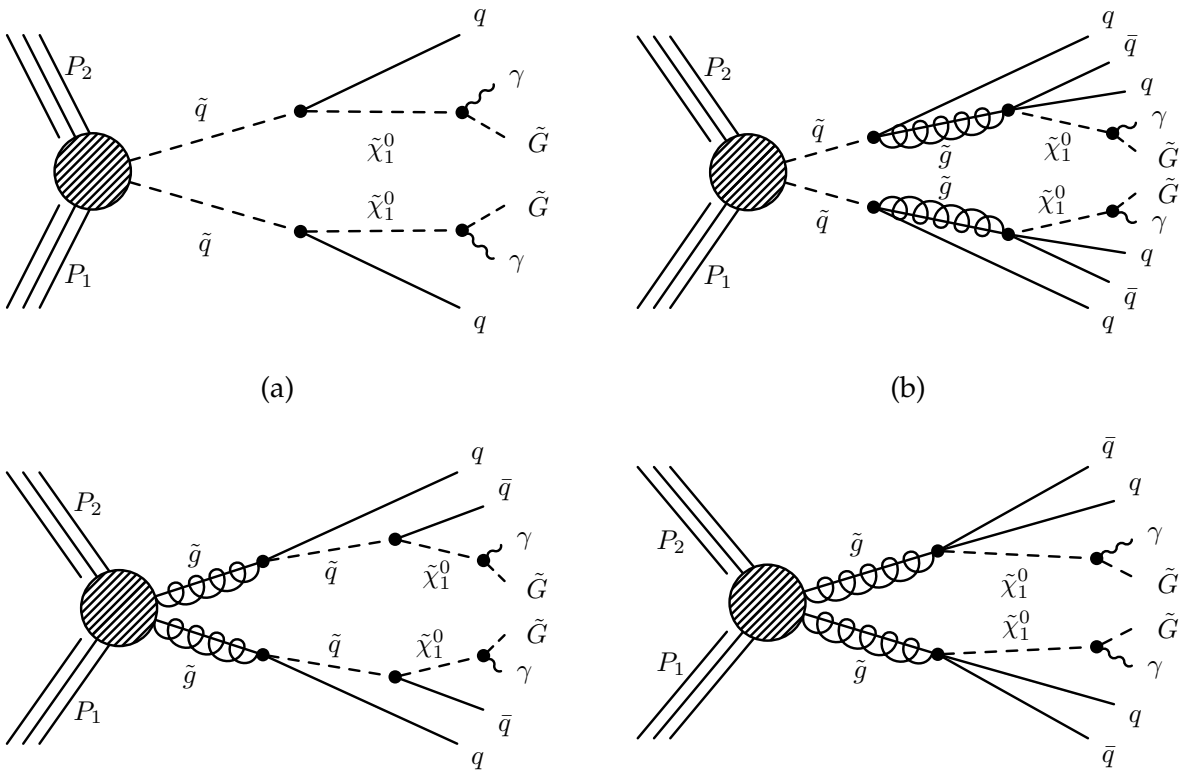

Figure 5: Feynman diagram for (a) squark-squark production, (b) squark-squark decaying through gluino-gluino, and (c) gluino-gluino decaying through squark-squark in the squark-gluino model and (d) for gluino-gluino in the simplified model T5gg.

In order to derive a limit on a given SUSY model, we use the LHC CL_s procedure [40]. The signal plus background likelihood function is defined by adding the signal comonent to the background component. Additional systematic effects to the normalization and the shape are modeled as log-normal systematics. The dependence of the likelihood on the nuisance parameters is removed through profiling. The ratio of the profiled likelihoods for the two hypotheses (σ fixed to the value under test versus $\hat{\sigma}$ obtained by maximizing the likelhiood, with $0 < \hat{\sigma} < \sigma$) is used as the test statistic to associate a CL_s value to each value of σ.

Fig 6 shows the excluded region in the ($m_{\tilde{g}}$, $m_{\tilde{q}}$) plane for the squark-gluino model, and the ($m_{\tilde{g}}$, $\tilde{\chi}_1^0$) plane for T5gg. The red (black) dashed line shows the expected (observed) limit. The thin dashed line and band show the 68% range about the expected limit. The solid line quantifies the impact of the theoretical uncertainty in the cross section on the observed limit. The color code of the temperature plot shows the excluded cross section for each set of mass values.

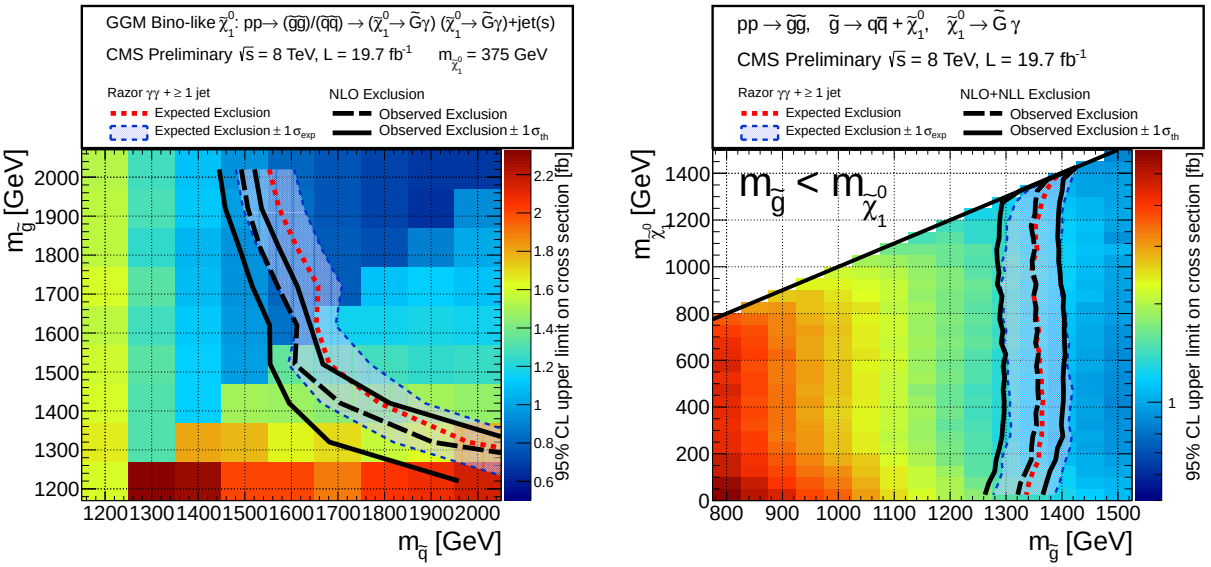

(a) (b)

Figure 6: Excluded mass region for (a) squark-gluino model and (b) T5gg. The red (black) dashed line shows the expected (observed) limit. The thin dashed blue line and band show the 68% range about the expected limit. The black solid line quantifies the impact of the theoretical uncertainty in the cross section on the observed limit. The color code to the right of the figure shows the excluded cross section for each set of mass values.

8 Conclusions

A search for supersymmetry in events with at least two photons and at least one jet is performed on pp collisions at $\sqrt{s} = 8$ TeV. The signal is characterized as as a wide bump in the distribution of the razor kinematic variable M_R, for events with large values of the razor ratio R^2. The signal is determined in a control region at low R^2 and extrapolated in the signal region. No excess is observed. The result is interpreted in terms of exclusion limits on squark and gluinos in GGM-inspired SMS. For comparable parameter space between the GGM and T5gg SMS, the T5gg SMS has a lower expected upper limit due to the 100 % branching fraction of the neutralino decay.

References

[1] J. Wess and B. Zumino, "Supergauge Transformations in Four-Dimensions", *Nucl. Phys. B* **70** (1974) 39, doi:10.1016/0550-3213(74)90355-1.

[2] Y. Golfand and E. Likhtman, "Extension of the Algebra of Poincare Group Generators and Violation of p Invariance", *JETP Lett.* **13** (1971) 323.

[3] D. Volkov and V. Akulov, "Possible universal neutrino interaction", *JETP Lett.* **16** (1972) 438.

[4] A. H. Chamseddine, R. L. Arnowitt, and P. Nath, "Locally supersymmetric grand unification", *Phys. Rev. Lett.* **49** (1982) 970, doi:10.1103/PhysRevLett.49.970.

[5] G. L. Kane, C. F. Kolda, L. Roszkowski, and J. D. Wells, "Study of constrained minimal supersymmetry", *Phys. Rev. D* **49** (1994) 6173, doi:10.1103/PhysRevD.49.6173, arXiv:hep-ph/9312272.

[6] P. Fayet, "Supergauge invariant extension of the Higgs mechanism and a model for the electron and its neutrino", *Nucl. Phys. B* **90** (1975) 104, doi:10.1016/0550-3213(75)90636-7.

[7] R. Barbieri, S. Ferrara, and C. A. Savoy, "Gauge models with spontaneously broken local supersymmetry", *Phys. Lett. B* **119** (1982) 343, doi:10.1016/0370-2693(82)90685-2.

[8] L. J. Hall, J. D. Lykken, and S. Weinberg, "Supergravity as the messenger of supersymmetry breaking", *Phys. Rev. D* **27** (1983) 2359, doi:10.1103/PhysRevD.27.2359.

[9] P. Ramond, "Dual theory for free fermions", *Phys. Rev. D* **3** (1971) 2415, doi:10.1103/PhysRevD.3.2415.

[10] P. Fayet, "Mixing Between Gravitational and Weak Interactions Through the Massive Gravitino", *Phys. Lett.* **B70** (1977) 461, doi:10.1016/0370-2693(77)90414-2.

[11] H. Baer, M. Brhlik, C. H. Chen, and X. Tata, "Signals for the Minimal Gauge-Mediated Supersymmetry Breaking Model at the Fermilab Tevatron Collider", *Phys. Rev.* **D55** (1997) 4463, doi:10.1103/PhysRevD.55.4463.

[12] H. Baer, P. G. Mercadante, X. Tata, and Y. L. Wang, "Reach of Tevatron Upgrades in Gauge-Mediated Supersymmetry Breaking Models", *Phys. Rev.* **D60** (1999) 055001, doi:10.1103/PhysRevD.60.055001.

[13] S. Dimopoulos, S. Thomas, and J. D. Wells, "Sparticle Spectroscopy and Electroweak Symmetry Breaking with Gauge-Mediated Supersymmetry Breaking", *Nucl. Phys.* **B488** (1997) 39, doi:10.1016/S0550-3213(97)00030-8.

[14] J. R. Ellis, J. L. Lopez, and D. V. Nanopoulos, "Analysis of LEP Constraints on Supersymmetric Models with a Light Gravitino", *Phys. Lett.* **B394** (1997) 354, doi:10.1016/S0370-2693(97)00019-1.

[15] M. Dine, A. Nelson, Y. Nir, and Y. Shirman, "New Tools for Low Energy Dynamical Supersymmetry Breaking", *Phys. Rev.* **D53** (1996) 2658, doi:10.1103/PhysRevD.53.2658.

[16] G. F. Giudice and R. Rattazzi, "Gauge-Mediated Supersymmetry Breaking", in *Perspectives on Supersymmetry*, p. 355. World Scientific, Singapore, 1998.

[17] P. Meade, N. Seiberg, and D. Shih, "General Gauge Mediation", *Prog. Theor. Phys. Suppl.* **177** (2009) 143, doi:10.1143/PTPS.177.143.

[18] M. Buican, P. Meade, N. Seiberg, and D. Shih, "Exploring General Gauge Mediation", *JHEP* **0903** (2009) 016, doi:10.1088/1126-6708/2009/03/016.

[19] CMS Collaboration, "Search for supersymmetry in events with photons and missing energy", CMS Physics Analysis Summary SUS-12-018, 2012.

[20] T. A. collaboration, "Search for Diphoton Events with Large Missing Transverse Momentum in 8 TeV pp Collision Data with the ATLAS Detector",.

[21] C. Rogan, "Kinematics for new dynamics at the LHC", (2010). arXiv:1006.2727. CALT-68-2790.

[22] CMS Collaboration, "Inclusive search for squarks and gluinos in pp collisions at $\sqrt{s} = 7$ TeV", *Phys. Rev. D* **85** (2012) 012004, doi:10.1103/PhysRevD.85.012004, arXiv:1107.1279.

[23] J. Alwall, P. Schuster, and N. Toro, "Simplified models for a first characterization of new physics at the LHC", *Phys. Rev. D* **79** (2009) 075020, doi:10.1103/PhysRevD.79.075020, arXiv:0810.3921.

[24] J. Alwall, M.-P. Le, M. Lisanti, and J. G. Wacker, "Model independent jets plus missing energy searches", *Phys. Rev. D* **79** (2009) 015005, doi:10.1103/PhysRevD.79.015005, arXiv:0809.3264.

[25] D. S. Alves, E. Izaguirre, and J. G. Wacker, "Where the sidewalk ends: jets and missing energy search strategies for the 7 TeV LHC", *JHEP* **10** (2011) 012, doi:10.1007/JHEP10(2011)012, arXiv:1102.5338.

[26] LHC New Physics Working Group Collaboration, "Simplified models for LHC new physics searches", *J. Phys. G* **39** (2012) 105005, doi:10.1088/0954-3899/39/10/105005, arXiv:1105.2838.

[27] CMS Collaboration, "Updated measurements of the Higgs Boson at 125 GeV in the two photon decay channel", CMS Physics Analysis Summary HIG-13-001, 2013.

[28] CMS Collaboration, "Commissioning of the Particle-Flow reconstruction in Minimum-Bias and Jet Events from pp Collisions at 7 TeV", CMS Physics Analysis Summary PFT-10-002, 2010.

[29] CMS Collaboration, "Isolated Photon Reconstruction and Identification at sqrts", CMS Physics Analysis Summary EGM-10-006, 2011.

[30] M. Cacciari, G. P. Salam, and G. Soyez, "The Anti-k(t) jet clustering algorithm", *JHEP* **0804** (2008) 063, doi:10.1088/1126-6708/2008/04/063, arXiv:0802.1189.

[31] M. Cacciari, G. P. Salam, and G. Soyez, "FastJet User Manual", *Eur.Phys.J.* **C72** (2012) 1896, doi:10.1140/epjc/s10052-012-1896-2, arXiv:1111.6097.

[32] S. Hoeche et al., "Matching parton showers and matrix elements", (2006). arXiv:hep-ph/0602031.

[33] CMS Collaboration, "The fast simulation of the CMS detector at LHC", *J. Phys. Conf. Ser.* **331** (2011) 032049, doi:10.1088/1742-6596/331/3/032049.

[34] W. Beenakker, R. Höpker, M. Spira, and P. M. Zerwas, "Squark and gluino production at hadron colliders", *Nucl. Phys. B* **492** (1997) 51, doi:10.1016/S0550-3213(97)80027-2, arXiv:hep-ph/9610490.

[35] A. Kulesza and L. Motyka, "Threshold resummation for squark-antisquark and gluino-pair production at the LHC", *Phys. Rev. Lett.* **102** (2009) 111802, doi:10.1103/PhysRevLett.102.111802, arXiv:0807.2405.

[36] A. Kulesza and L. Motyka, "Soft gluon resummation for the production of gluino-gluino and squark-antisquark pairs at the LHC", *Phys. Rev. D* **80** (2009) 095004, doi:10.1103/PhysRevD.80.095004, arXiv:0905.4749.

[37] W. Beenakker et al., "Soft-gluon resummation for squark and gluino hadroproduction", *JHEP* **12** (2009) 041, doi:10.1088/1126-6708/2009/12/041, arXiv:0909.4418.

[38] W. Beenakker et al., "Squark and gluino hadroproduction", *Int.J.Mod.Phys. A* **26** (2011) 2637, doi:10.1142/S0217751X11053560, arXiv:1105.1110.

[39] M. Krämer et al., "Supersymmetry production cross sections in pp collisions at $\sqrt{s} = 7$ TeV", (2012). arXiv:1206.2892.

[40] CMS and ATLAS Collaboration Collaboration, "Procedure for the LHC Higgs boson search combination in Summer 2011 ", CMS Physics Analysis Summary CMS-NOTE-2011-005, 2011.

A Signal Selection Event Yields

Cut	T5gg [GeV] $m_{\tilde{g}} = 1350$ $m_{\tilde{\chi}_1^0} = 75$	T5gg [GeV] $m_{\tilde{g}} = 1350$ $m_{\tilde{\chi}_1^0} = 375$	T5gg [GeV] $m_{\tilde{g}} = 1350$ $m_{\tilde{\chi}_1^0} = 1275$	GGM [GeV] $m_{\tilde{q}} = 2000$ $m_{\tilde{g}} = 1320$	GGM [GeV] $m_{\tilde{q}} = 1500$ $m_{\tilde{g}} = 2020$
None	25.6 ± 0.3	25.6 ± 0.3	25.6 ± 0.3	33.7 ± 0.3	24.0 ± 0.2
2 $\gamma\gamma$	12.6 ± 0.2	14.7 ± 0.2	16.5 ± 0.2	12.6 ± 0.2	11.7 ± 0.2
1 loose jet	12.4 ± 0.2	14.4 ± 0.2	15.3 ± 0.2	12.2 ± 0.2	11.4 ± 0.2
Baseline Razor	11.4 ± 0.2	13.8 ± 0.2	15.1 ± 0.2	11.6 ± 0.2	10.9 ± 0.2
Signal Region	10.0 ± 0.2	12.6 ± 0.2	14.9 ± 0.2	10.6 ± 0.2	10.2 ± 0.2
$M_R > 1.5$ TeV	7.9 ± 0.1	9.6 ± 0.2	9.6 ± 0.2	7.6 ± 0.2	8.8 ± 0.1
$R^2 > 0.04$	5.5 ± 0.1	7.3 ± 0.1	9.0 ± 0.2	5.6 ± 0.1	7.2 ± 0.1

Figure 7: An example signal event yield for 19.7 fb^{-1} is shown for three T5gg mass points and two GGM mass points. The points are selected to be near the exclusion limit. The baseline razor selection includes $M_R > 600$ GeV and $R^2 > 0.01$. The signal region additionally requires $R^2 > 0.02$. All errors are statistical and all masses are in GeV.